THE JOURNAL OF PHYSICAL CHEMISTRY C
A JOURNAL OF THE AMERICAN CHEMICAL SOCIETY
pubs.acs.org/JPCC
Article

Solids with Two Mobile Ions: Proton H^+ Self-Diffusion in Li–H Exchanged Garnet-Type $Li_6La_3ZrTaO_7$ as Seen by Solid-State ^1H NMR Relaxation

Maria Gombotz, Caroline Hiebl, Florian Stainer, and H. Martin R. Wilkening*

Cite This: J. Phys. Chem. C 2023, 127, 10960–10967
Read Online

ABSTRACT: The development of ceramic proton conductors is currently attracting great attention, as they might be useful to construct new energy storage systems. $Li_6La_3ZrTaO_{12}$ (LLZTO) is known for its rapid Li^+ diffusivity as has been directly revealed by ^7Li NMR measurements. Exchanging parts of the highly mobile Li^+ ions by protons through treatment of a single crystal in water or glacial acetic acid yields a mixed proton–lithium ionic conductor. Here, H^+ proton diffusivity and Li^+ diffusivity have separately been studied with element-specific ^1H and ^7Li NMR spectroscopy. While long-range ^7Li diffusion is noticeably slowed in Li–H exchanged LLZTO, we directly observe rather high H^+ diffusivity, which is, however, significantly slower than Li^+ dynamics. With the help of spin–lattice relaxation measurements we were able to measure local (and long-range) energy barriers (0.20(1) eV vs 0.45(3) eV) as well as the self-diffusion coefficient D_H of H^+ dynamics (1.2×10^{-15} m^2 s^{-1} at 125 °C). These encouraging results are assumed to open new directories in designing ceramics offering fast transport pathways for protons.

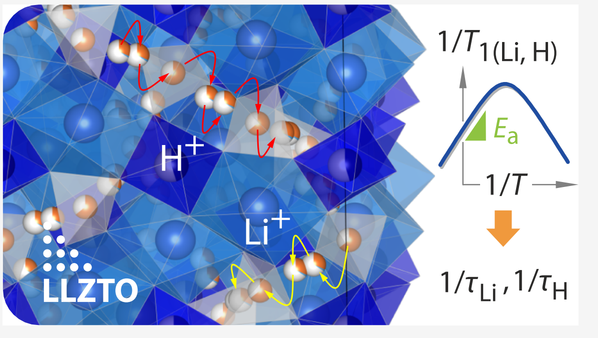

■ INTRODUCTION

Solids with mobile ions, such as H^+, Li^+, Na^+, Ag^+, F^-, and O^{2-}, play a pivotal role in materials science[1] for a range of applications.[2−6] In particular, they are needed to realize all-solid-state lithium and sodium batteries[7−13] and to develop oxide fuel cells.[4,14−16] The search for proton conductors[5,6,17,18] to develop proton conducting fuel cells has also reached a rather high level. Classical proton conducting ceramics[5,18,19] include oxides such as alkaline earth cerates and zirconate perovskites based on acceptor-doped $SrCeO_3$, $BaCeO_3$, $SrZrO_3$, and $BaZrO_3$ and other compounds such as CsH_2PO_4.[6,20−31] Usually, protons are incorporated in, e.g., $BaZrO_3$ by treatment with water vapor or H_2 gas. Recently, it has been shown that the exact proton concentration in Y-doped $BaZrO_3$ sensitively affects H^+ conductivities involving nanoscale percolation pathways with low dimensionality.[32]

From an application point of view, suitable proton conductors should not only possess a high H^+ conductivity, they must also be chemically stable under the fuel cell operating conditions and allow for low-cost manufacturing. In addition, in many cases long-range proton conduction is blocked at the grain boundary regions in polycrystalline materials. Hence, the search for new materials attracts great interest.

Here, we investigated whether the well-known garnet-type Li^+ ion conductor $Li_6La_3ZrTaO_{12}$ (LLZTO, see Figure 1), which is based on $Li_6La_3Zr_2O_{12}$ (LLZO), could indeed act as a promising H^+ ion conductor[17] at least if we restrict ourselves to bulk properties. For this purpose, we prepared Li–H exchanged LLZTO powder samples by treating the garnet samples in water or glacial acetic acid. To separately study H^+ and Li^+ ion dynamics, we took advantage of element-specific nuclear magnetic resonance (NMR) spectroscopy. As outlined in detail elsewhere (see also the Supporting Information),[33−36] the measurement of diffusion-controlled ^1H and ^7Li NMR spin–lattice relaxation rates and NMR spectra provided direct insights into the motional processes from an atomic point of view. NMR is a contactless, that is, a noninvasive, method highly useful to directly probe ion dynamics on the angstrom length scale.[34] Indeed, H-bearing LLZTO turned out to be a suitable model system to measure proton jump activation energies E_a and proton self-diffusion coefficients D_H at temperatures as low as 125 °C.

The crystal structure of LLZTO is depicted in Figure 1. It crystallizes with space group $Ia\bar{3}d$. The Li ions are distributed over several crystallographic sites, viz. 24*d* and 96*h*. These sites are partially occupied by the cations whereby H^+ are expected

Received: April 7, 2023
Revised: May 16, 2023
Published: June 3, 2023

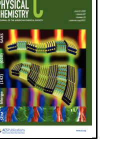

https://doi.org/10.1021/acs.jpcc.3c02330
J. Phys. Chem. C 2023, 127, 10960−10967

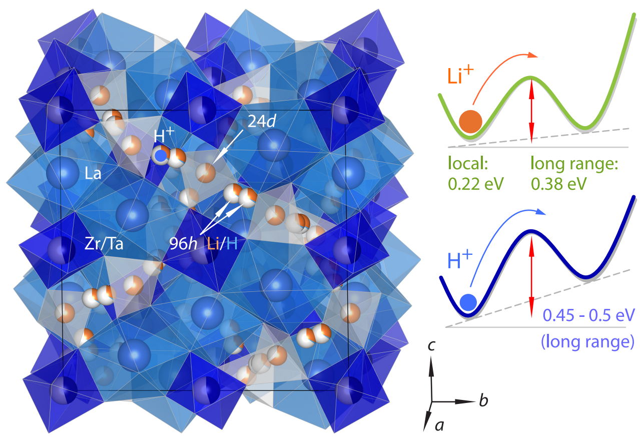

Figure 1. Left: crystal structure of LLZTO adopting cubic symmetry ($Ia\bar{3}d$, no. 230). Oxygen anions are omitted for clarity reasons. Li^+ transport takes advantage of a partially occupied Li sublattice comprising the sites 24*d* and 96*h*. Depending on the exact Li−H exchange process, protons occupy the same sites or a split site between these two. Right: schematic illustration of the hopping barriers (in eV) measured in this study.

to reside on the 96*h* positions. Recent neutron diffraction studies have, however, refined this "standard" picture revealing that the protons incorporated into LLZTO single crystals do, depending on the exact space group, occupy a so-called split site near 24*d*, which is also close to 96*h*.[37]

In general, $Li_7La_3Zr_2O_{12}$-type garnets (LLZO)[38] are widely considered as promising solid electrolytes for Li-based all-solid-state batteries.[39] In contact with H_2O and CO_2 the garnet LLZO forms a rather resistive Li_2CO_3 surface layer that might block the facile Li^+ transport across the electrolyte−electrode interface.[40] Hence, studying the formation of carbonates, which involves the Li^+−H^+ exchange reaction, has attracted great interest.[41] It has been reported that even garnets, which are stored in Ar-filled glove boxes, show the formation of Li_2CO_3.[42] These degradation processes are expected to also influence the implementation of garnets as ceramic electrolytes in Li-based batteries.

The Li^+−H^+ exchange reaction has been the subject of various earlier studies, which focused on a range of compounds[17] such as $Li_{7-x}H_xLa_3Sn_2O_{12}$,[43,44] Nb-containing $Li_7La_3Zr_2O_{12}$,[45] $Li_5La_3Nb_2O_{12}$,[46−48] the Ta-bearing oxides $Li_7La_3Zr_2O_{12}$,[49] and $Li_{6.5}La_3Zr_{1.5}Ta_{0.5}O_{12}$,[50] as well as $Li_{6-x}H_xCaLa_2Nb_2O_{12}$,[51] and $Li_{7-x}H_xLa_3Zr_2O_{12}$.[52] It turned out that garnets with a lithium content above three Li ions per formula unit $Li_3B_2C_3O_{12}$ (B and C elements with oxidation numbers +3 and +4)[43] are especially prone to the exchange of Li^+ ions by H^+ ions. Apart from this feature, local structures, chemical compositions, and the choice of doping elements seem to affect the cation exchange reaction, as has been reported for Al-doped LLZO,[53] $Li_{7-x}La_3(Zr, Ta)_2O_{12}$,[42] and $Li_5La_3Nb_2O_{12}$.[48] In another example, Sn-bearing tetragonal $Li_{7-x}H_xLa_3Sn_2O_{12}$ converted into its cubic form[43] upon H^+ insertion.

The extent of the exchange reaction does not only depend on the kind of treatment, which is usually performed with acids as reported in several studies,[47,48,54,55] but does also depend sensitively on the surface area exposed to, e.g., humid air or H_2O. The latter relationship has been studied by Yow et al.[49] The authors immersed a dense $Li_{6.6}La_3Zr_{1.6}Ta_{0.4}O_{12}$ pellet in

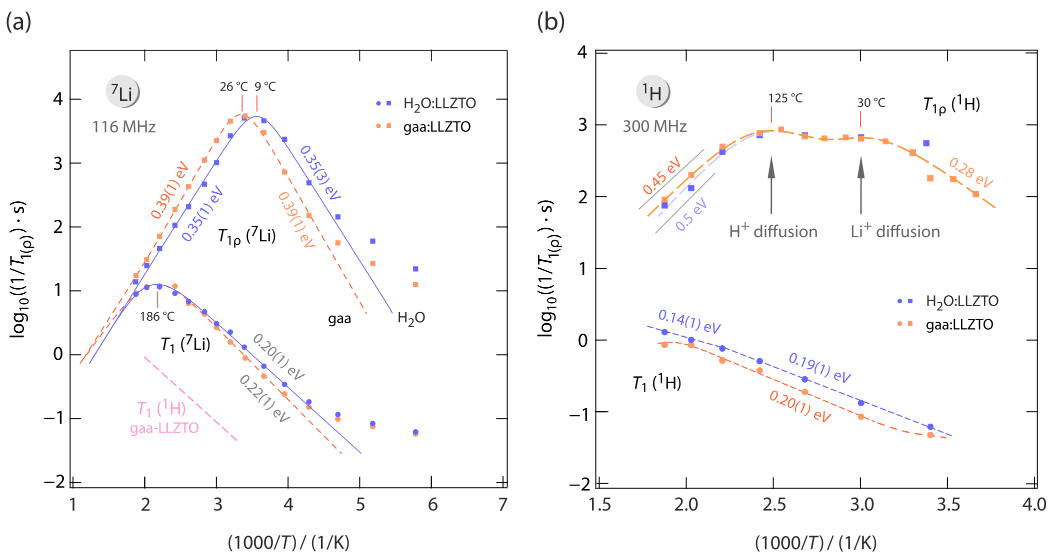

Figure 2. (a) ^{7}Li NMR spin−lattice relaxation rates recorded in both the laboratory frame (116 MHz; $1/T_1$) and rotating frame of reference (116 MHz, 20 kHz; $1/T_{1\rho}$). Data points refer to polycrystalline LLZTO samples treated in either water or glacial acetic acid (gaa). As compared to untreated LLZTO (see Figure S1), the rate peaks $1/T_1(1/T)$ reveal a light decrease in Li^+ diffusivity in LLZTO if protons had been incorporated. The corresponding spin-lock peak of untreated, H-free LLZTO appears at almost the same temperature as that of belonging to H_2O-LLZTO (see Figure S1). Dashed and solid lines show joint fits with BPP-type spectral density functions yielding activation energies (as indicated), Arrhenius prefactors, and asymmetry parameters (see Tables S1 and S2). (b) While, below approximately 500 K, the corresponding ^{1}H NMR rates $1/T_1$ (300 MHz) follow the same temperature behavior as the ^{7}Li NMR rates, the ^{1}H NMR spin-lock rates $1/T_{1\rho}$ (300 MHz, 20 kHz) pass through two shallow, diffusion-induced rate peaks. Disregarding absolute values, which are expected to be different for the rates $1/T_{1(\rho)}$ of the two nuclei, the peak appearing at lower temperature (30 °C) perfectly agrees with that the ^{7}Li NMR rates pass through (26 °C), pointing to the fact that ^{1}H NMR indirectly senses the ^{7}Li spin fluctuations (see text). Importantly, the peak showing up at higher temperature (125 °C) is interpreted to be directly caused by H^+ translational jump dynamics. This view is corroborated by our ^{1}H NMR line shape analysis.

https://doi.org/10.1021/acs.jpcc.3c02330
J. Phys. Chem. C 2023, 127, 10960−10967

water and reached an exchange level of 8.8% after 7 days, whereas for a powdered sample a value of 54.3% was obtained. Because the surface-to-bulk ratio plays a significant role, we used finely ground samples for the exchange reactions.

So far, the effect of Li−H exchange on ion dynamics has been studied by conductivity measurements[44,46,49,56] yielding, however, no clear-cut relationship between overall conductivity and the degree of proton exchange. NMR, on the other hand, is in principle capable to separately study H^+ dynamics and Li^+ diffusivity, as has been outlined above.

■ METHODS

Details of sample preparation and structural characterization by neutron diffraction of the $Li_6La_3ZrTaO_{12}$ single crystals, which served as starting material for the present study, have been published elsewhere[57] (see also the Supporting Information). Here, two pieces of $Li_6La_3ZrTaO_{12}$ single crystals were finely ground and immersed for 7 h either in distilled water (H_2O) or in glacial acetic acid (gaa, CH_3COOH). Afterward, the crushed powders were dried in air and then packed in NMR glass tubes (approximately 3 cm in length and 4 mm in diameter). An ICP OES (inductively coupled plasma optical emission spectrometry) study on the Li−H exchanged samples yields a composition of $Li_{5.6}H_xLa_3Zr_{0.9}Ta_{1.1}O_{12}$ with x = 0.3. As mentioned above, structural details of H-LLZTO, especially on the positions occupied by H in the garnet structure, have been reported in the literature recently.[37]

^{1}H (spin quantum number I = 1/2) and ^{7}Li (I = 3/2) spectra as well as the corresponding NMR spin−lattice relaxation rates were recorded in the laboratory frame of reference ($1/T_1$) as well as in the rotating frame of reference ($T_{1\rho}$)[11,58] with a Bruker Avance III NMR spectrometer operating at a nominal magnetic field of 7.04 T yielding Larmor frequencies $\omega_0/2\pi$ of 300 MHz for ^{1}H and 116.59 MHz for ^{7}Li. A commercial ceramic probe (Bruker BioSpin) was used to carry out variable temperature measurements from 173 up to 533 K. For the measurements in the rotating frame of reference, the locking frequency was adjusted to $\omega_1/2\pi \approx 20$ kHz. We used the classical saturation recovery pulse sequence to record the $1/T_1$ rates and the spin-lock technique to measure the rates $T_{1\rho}$. Details of the exact setup can be found in earlier studies of our group.[35,58,59] Here, the 90° pulse lengths varied from 2 to 2.5 μs. Locking pulses at lower power were chosen such that the whole transients could be measured. As described elsewhere, we used stretched exponential functions to parametrize the magnetization curves. ^{7}Li and ^{1}H NMR free induction decays were recorded with a single 90° pulse and proper recycle delay of at least $5T_1$; Fourier transformation directly yielded the spectra shown here focusing, in the case of ^{7}Li NMR on central transitions ($\pm1/2$, $\mp1/2$) only. Full ^{7}Li NMR spectra including the quadrupole satellite transitions of LLZO-type (single-crystalline) samples are shown elsewhere.[60]

■ RESULTS AND DISCUSSION

In Figure 2, the results from ^{1}H and ^{7}Li NMR spin−lattice relaxation measurements are shown. At sufficiently high temperatures, the rates are purely induced by diffusion (diff) ($1/T_{1(\rho)} = 1/T_{1(\rho),\mathrm{diff}}$); any nondiffusive background effects are completely absent for T > 250 K (T_1) and for T > 215 K ($1/T_{1(\rho)}$). The ^{7}Li NMR rates of the two samples investigated show the expected behavior for Li self-diffusion in garnets. While the $1/T_1(1/T)$ peak is sensitive to Li^+ dynamics with motional correlation rates $1/\tau_c$ on the megahertz to gigahertz time scale, the corresponding spin-lock NMR peak $1/T_{1(\rho)}(1/T)$ Li^+ captures motional processes on the kilohertz time scale.

The lines in Figure 2 represent fits with a so-called modified BPP-type[34,61,62] spectral density function J

$$J(\omega_{0(1)}) \propto 1/T_{1(\rho)} = C''_{0(1)}\frac{\tau_c}{1 + (2\omega_{0(1)}\tau_c)^\beta} \quad (1)$$

that yields the (microscopic) activation energy E_a and the Arrhenius prefactor τ_{c0}^{-1} included in

$$\tau_c^{-1} = \tau_{c0}^{-1}\exp(-E_a/k_BT) \quad (2)$$

where k_B denotes Boltzmann's constant. E_a refers to the slope of the high-temperature flank of the peaks in Figure 2. In general, in this T regime $\omega_{0(1)}\tau_c \ll 1$ is valid, and NMR captures many spin fluctuations during a single spin precession, thus being sensitive to Li^+ jump processes on a rather longer length scale as compared to what NMR senses in the low-T regime ($\omega_{0(1)}\tau_c \gg 1$).[34,62] These activation energies, $E_{a,\mathrm{low}}$, extracted directly from the low-T flank are included in Figure 2 as well. Especially for $1/T_1(1/T)$, we see that rather low activation energies are obtained (0.22 and 0.20 eV), which characterize local ion dynamics[59,62] in H-bearing LLZTO. For comparison, in H-free LLZTO single crystals we obtained 0.24 eV,[57] which is quite comparable to the values for the Li−H exchanged samples (see below).

In general, the so-called asymmetry parameter β (see eq 1[34]) links E_a with $E_{a,\mathrm{low}}$ according to

$$E_{a,\mathrm{low}} = (1-\beta)E_a \quad (3)$$

β = 2, which is the simple BPP case for uncorrelated motion, would lead to fully symmetric rate peaks as is indeed seen for $1/T_{1(\rho)}$ of gaa-LLZTO (see Figure 2 and below). In general, β characterizes the frequency dependence of the relaxation rate in the low-T limit ($\omega_{0(1)}\tau_c \gg 1$): $1/T_{1(\rho)} \propto \omega_{0(1)}^{\beta}$; for comparison, in the limit $\omega_{0(1)}\tau_c \ll 1$ we have to deal with $1/T_{1(\rho)} \neq f(\omega_{0(1)})$ as far as 3D diffusion is considered.[34,35] A detailed discussion and list of the fitting parameters are provided in the Supporting Information (see Tables S1 and S2), which also briefly summarizes the basics behind relaxation NMR based on several textbooks.

As is well documented in the literature by us,[57] the ^{7}Li NMR spin−lattice relaxation rates ($1/T_1$) of untreated, that is, H-free, single-crystalline LLZTO pass through a rate peak located at T_{max} = 434 K (161 °C, see Figure S1). At T_{max} the conditions

$$\omega_0\tau_c \approx 1 \text{ and } \omega_1\tau_c \approx 0.5 \quad (4)$$

are valid, which allow direct access to the motional correlation rate $1/\tau_c$.[34,57] $\omega_0\tau_c \approx 1$ refers to a single spectral density term J; taking into account two terms (see the Supporting Information), in the case of dipolar interactions we have $\omega_0\tau_c \approx 0.62$. Any shift of the $1/T_{1(\rho)}$ rate peak toward lower or higher temperatures directly indicates an increase or decrease of Li^+ diffusivity. Here, independent of the treatment procedure, Li−H exchange shifts this peak to higher temperatures (T_{max} = 459 K (186 °C)), indicating that H incorporation has a slightly detrimental effect on (local) Li diffusivity (see Figure S1), to which $1/T_1$ is primarily sensitive. It does for sure not increase the already rapid Li^+ exchange

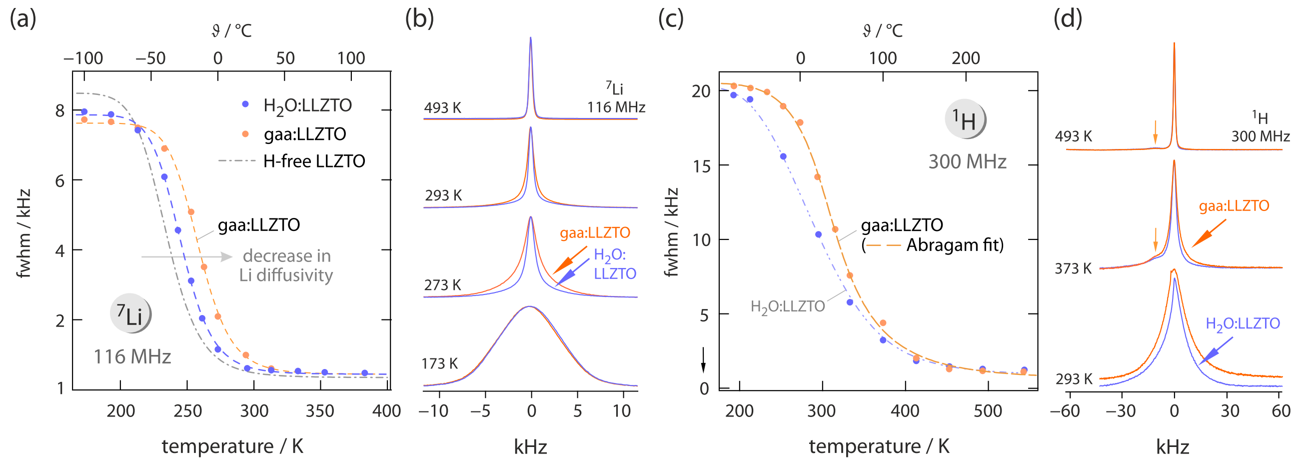

Figure 3. (a) Change of the ^{7}Li NMR line widths of LLZTO treated either in water (H_2O:LLZTO) or in glacial acetic acid (gaa:LLZTO). The dashed-dotted line illustrates the motional narrowing curve belonging to untreated H-free LLZO. In general, the shift of the inflection point of the curve toward higher T points to less mobile Li ions. The lines are to guide the eye. (b) ^{7}Li NMR lines used to extract the widths shown in (a); temperatures at which the spectra have been recorded are indicated. The original Gaussian-shaped line changes into a Lorentzian one upon heating. On the temperature scale, the averaging process sets in a bit earlier for H_2O:LLZTO, see also (a). (c) ^{1}H NMR motion-induced line narrowing curves. For gaa-LLZTO the inflection point of the curve is located at $T_i \approx 320$ K, which is higher than that of the corresponding ^{7}Li NMR curve ($T_i \approx 260$ K indicating still faster ^{7}Li diffusion in gaa-LLZTO.) The dashed line uses an Abragam fit to guide the eye (see text). (d) ^{1}H NMR lines of gaa:LLZTO and H_2O:LLZTO.

processes involving the sites 24*d* and 96*h*.[60] As mentioned above, $E_{a,low}(T_1)$ remains almost unaffected by Li−H exchange.

This situation of having two mobile ionic species resembles the situation in mixed alkali glasses showing a pronounced decrease in ionic conductivity[63,64] and ionic diffusivity as probed by NMR, for example,[65] upon admixing a foreign mobile cation. Here, however, such a process is seen on the angstrom length scale. Though the current decrease is measurable, it is much less pronounced than in mixed-alkali glasses. It is even less pronounced if we consider ^{7}Li translational dynamics probed on longer time scales as revealed by the variable-temperature spin-lock experiments measuring $1/T_{1(\rho)}(1/T)$.

For the corresponding rate peaks $1/T_{1\rho}(1/T)$, recorded in the rotating frame of reference (20 kHz locking frequency), we observe that the peak referring to LLZTO treated in water T_{max} = 282 K (9 °C) is within errors and sample-to-sample variations, comparable to that of the untreated H-free material for which the peak appears at T_{max} = 286 K (13 °C) (see Figure S1).[57] A larger shift in $1/T_{1(\rho)}(1/T)$ is, however, seen for the sample immersed in glacial acetic acid (T_{max} = 299 K (26 °C)), revealing a decrease in long-range Li^+ self-diffusivity upon H^+/Li^+ exchange (see below). Compared to untreated LLZO, we also observe a change in shape of the peak (see Figure S1); the originally asymmetric rate peak of H-free LLZTO (β = 1.46) turns into a symmetric one, as is clearly indicated by the asymmetry parameters β: According to our analysis with the modified BBP-type relaxation functions (see eq 1), for H_2O-LLZTO and gaa-LLZTO the best fits yield β = 2 for each peak (see Table S2). Interestingly, this counter-intuitive result is surprising as we would have expected stronger correlation effects influencing ion dynamics with rates in the kilohertz regime in systems with two mobile species (see above).

In Figure 2b the ^{1}H NMR rates $1/T_1$ are shown, which are as compared to the corresponding ^{7}Li data, shifted toward lower absolute values because of weaker spin−spin couplings described by C' in eq 1. Though shifted, they follow the same trend as the ^{7}Li NMR rates; see the dashed line in Figure 2 which runs in parallel to the low-temperature flank of the $1/T_1(^7\text{Li})(1/T)$ peak. The flank yields an activation energy of approximately 0.2 eV, which again characterizes local H^+ jump processes in LLZTO. Because of the similarities in activation energies, we think that longitudinal proton relaxation can be indirectly induced by rapid Li^+ spin fluctuations of dipolar magnetic nature in the direct neighborhood of the ^{1}H spins.

Most importantly, for spin-lock ^{1}H NMR, an additional feature is observed that is absent in ^{7}Li NMR. Coming from low temperatures, the rates $1/T_{1\rho}(^1\text{H})$ pass through a shallow rate peak at ϑ = 30 °C. Again, we attribute this low-T peak to be caused by ^{7}Li spin fluctuations sensed by the ^{1}H spins located in the direct vicinity of the Li spins. Importantly, the ^{1}H spin-lock NMR rates $1/T_{1(\rho)}$ run through a *second* rate peak located at ϑ = 125 °C. Such a peak is clearly missing in ^{7}Li NMR. Its high-temperature flank points to an activation energy of 0.45 eV, which is identified as the barrier that characterizes long-range proton transport in H-bearing LLZTO. In general, at temperatures lower than T_{max}, we deal with $\omega_0\tau_c \gg 1$, and short-range ion motions are sampled on the low-T flank of a given $1/T_1(1/T)$ peak. For $T > T_{max}$, the condition $\omega_0\tau_c \ll 1$ holds, and many events are captured during a single spin precession, enabling access to long-range ion dynamics.[34]

The rates $1/T_{1\rho}(^1\text{H})$ turned out to be quite similar for the two samples investigated. To detect any significant differences the Li−H exchange procedure might have on H^+ diffusivity, we recorded ^{1}H NMR line shapes and followed the change of the central transition as a function of temperature. The results are together with those for ^{7}Li, shown in Figure 3.

At low temperatures, the dipolarly broadened ^{7}Li NMR central lines can be well described with Gaussian profiles and reveal a full width at half-height of approximately 8 kHz (see Figure 3a,b). As soon as diffusive motions of the Li ions reach correlation rates in the order of this rigid-lattice line width, the lines start to narrow because dipole−dipole interactions are increasingly averaged. In general, NMR line narrowing is sensitive to slower motional processes as those probed by 1/

https://doi.org/10.1021/acs.jpcc.3c02330
J. Phys. Chem. C 2023, 127, 10960−10967

$T_{1\rho}$.[34] Moreover, while in relaxation NMR (see above) both magnetic dipolar and electric qudrupolar interactions[35] could determine the rates, dipole−dipole interactions are mainly responsible for the line narrowing process in ^{7}Li NMR. Upon heating, this motion-induced averaging yields characteristic line narrowing curves, which are shown in Figure 3a. The inflection points of the curves on the temperature scale help compare the change in Li^+ diffusivity. For untreated LLZTO (see the dashed-dotted line), the temperature T_i of the inflection point is below 250 K whereas for H_2O-LLZTO we obtain T_i > 250 K; a further shift is seen for gaa-LLZTO. Undoubtedly, these changes reveal a noticeable decrease in long-range Li^+ diffusivity upon Li−H exchange, as has also been discussed by Aguadero and co-workers on the basis of impedance measurements.[56]

Most importantly, ^{1}H NMR does also reveal a significant narrowing of the corresponding resonances (see Figure 3c,d). Because of the rather strong ^{1}H−^{1}H dipolar interactions, the rigid line width ν_{rigid} turns out to be significantly larger than that seen in ^{7}Li NMR (8 kHz vs 20 kHz). Hence, in the case of ^{1}H NMR, motional averaging is expected to be slightly shifted toward higher temperatures as compared to the situation we met for ^{7}Li NMR. Here, the inflection point of the narrowing curve of gaa-LLZTO is given by $T_i \approx 325$ K (52 °C), clearly indicating rapid ^{1}H translational motions. Finally, these motions can fully average the homonuclear dipole−dipole interactions to which the ^{1}H spins are mainly exposed. The regime of extreme narrowing is almost reached at $T \approx 450$ K. At higher temperatures the width of the ^{1}H NMR line is simply determined by the inhomogeneity of the external magnetic field used to sample the lines. A rather sharp, fully narrowed ^{1}H NMR line is obtained at 493 K (see Figure 3d). For H_2O:LLZTO the results are quite similar, as already suggested by the $1/T_{1\rho}$ NMR rate measurements (see above). The final width in the order of 1000 Hz clearly suggests a mechanism that fully averages the prominent ^{1}H−^{1}H dipolar interactions. In our opinion, only rapid translational H^+ dynamics can be responsible for this observation. These translational dynamics might also enable long-range proton transfer as dipolar interactions cannot be effectively averaged by strictly localized hopping processes.

The tiny signal marked by vertical arrows in Figure 3d, as is seen for both samples, might point to an impurity phase or to H^+ ions residing on a different crystallographic position. As any coalescence effects are missing, no significant exchange between these H spins occurs on the NMR time scale. Most of the H spins are involved in the averaging process described by the motional curves shown in Figure 3c.

While the ^{7}Li NMR motional narrowing curves span a range of approximately Δ = 50 K between onset of narrowing and reaching the extreme narrowing regime (see Figure 3a), in the case of ^{1}H NMR the averaging process takes place over a large temperature range of Δ = 100 K pointing to a broader distribution of ^{1}H translational correlation rates. This idea is consistent with the rather broad $1/T_{1\rho}(^1\text{H})$ NMR rate peak seen in Figure 2b. The dashed line in Figure 3c represents a fit using the Abragram formalism.[66] In the presence of a broad distribution of motional correlation rates such an analysis does, however, underestimates the activation energy. Here, the Abragam analysis yields an activation energy of only 0.2 eV. For comparison, 0.3 eV is obtained if the Hendrickson−Bray equation[66] is used to analyze the change in line width as a function of temperature, also underestimating E_a obtained from spin-lock NMR probing long-range ion dynamics.

Finally, we can use the ^{1}H NMR $1/T_{1\rho}$ rate peak assigned to proton dynamics (see Figure 3b, T_{max} = 125 °C) to estimate the H diffusion coefficient in H-LLZTO (see Figure 4). At 125 °C the ^{1}H motional correlation rate $1/\tau_c$, which is expected to be equal to the jump rate $1/\tau$ within a factor of 2,[34] is given by $\tau_c \approx 0.5/\omega_1$. As a first approximation, for ω_1 we used the angular locking frequency ($\omega_1 = \nu_1 \times 2\pi$) instead of the usually unknown *effective* frequency[35] at the ^{1}H nuclear site. This effective frequency is, however, expected to be of the same order of magnitude as ω_1. In the present case we obtain $1/\tau_c(125\ °\text{C}) = 2.51 \times 10^5\ \text{s}^{-1}$. Assuming a mean jump distance in the order of 1.7 Å, we obtain a self-diffusion coefficient in the order of $D_H = 1.2 \times 10^{-15}\ \text{m}^2\ \text{s}^{-1}$ at 125 °C. According to Figure 2b, the activation energy for H^+ hopping takes a value of 0.45 eV. The same value is reached by Li^+ at much lower temperatures, namely at 30 °C (vide supra).

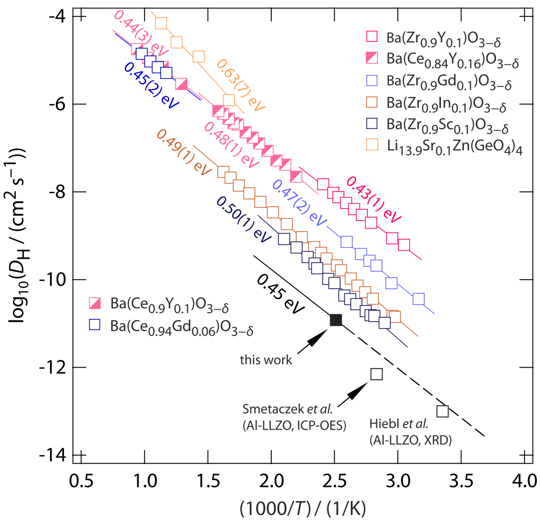

Figure 4. Comparison of the H^+ self-diffusion coefficient obtained in this work with those from Smetaczek et al.[67] and Hiebl et al.[53] on Al-containing $Li_6La_3Zr_2O_{12}$ (LLZO); see text for further details. For comparison, we have included tracer (pulsed field gradient NMR) or solid-state diffusion coefficients characterizing proton diffusivity in a range of other oxides based on, e.g., $Ba(Zr_{0.9}X_{0.1})O_{3-\delta}$ (X = Y, Gd, In, Sc) studied by Kreuer and co-workers,[68] $Ba(Ce_{0.84}Y_{0.16})O_{3-\delta}$,[69] $Ba(Ce_{0.9}Y_{0.1})O_{3-\delta}$,[70] $Ba(Ce_{0.94}Gd_{0.06})O_{3-\delta}$,[71] and $Li_{13.9}Sr_{0.1}Zn(GeO_4)_4$.[72] We refer to the literature for the exact compositions. For the sake of completeness, in Kreuer et al.[68] also compounds with even lower H diffusivities are discussed. The solid line referring to the data point of this work (LLZTO) corresponds to 0.45 eV as deduced from spin−lattice relaxation NMR. This activation energies are in excellent agreement with those of the $BaZrO_3$-based compounds shown.

In addition to evaluating the ^{1}H NMR relaxation rates, also the motional narrowing curve helps in supporting the D_H value determined. The estimated jump rate of $1/\tau$ ($\approx 1/\tau_c$) of $2.51 \times 10^5\ \text{s}^{-1}$ refers to approximately 400 K. Indeed, at this temperature, right at the beginning of the extreme narrowing regime, the motional narrowing curve of gaa-LLZTO suggests that $1/\tau$ should be equal to or higher than $\nu_{rigid} \times 2\pi \approx 1.25 \times 10^5\ \text{s}^{-1}$.

In Figure 4, we compare this H^+ diffusion behavior with those of other (ceramic) proton conductors[68−72] that are currently discussed in the literature (see above). The graph

https://doi.org/10.1021/acs.jpcc.3c02330
J. Phys. Chem. C 2023, 127, 10960−10967

does also contain (chemical) (inter)diffusion coefficients describing H dynamics in LLZO, which have been determined by means of single-crystal X-ray diffraction[53] as well as by ICP-OES; see the work by Fleig and co-workers.[67] Especially the latter coefficient represents a tracer diffusion coefficient D_T rather than a self-diffusion coefficient to which NMR relaxation is sensitive here.

CONCLUSION

Li−H exchanged LLZTO-based garnets offer a possibility to create ionic conductors with noticeable H^+ transport properties. Here, we used ^{1}H NMR (spin-lock) spin−lattice relaxation measurements and line shape analyses to verify proton diffusivity within the rigid oxide host lattice. Though largely influenced by rapid ^{7}Li hopping processes, which is especially true for ^{1}H NMR spin−lattice relaxation in the laboratory frame of reference, the spin-lock ^{1}H NMR rates pass through an additional rate peak at 125 °C which we attribute to proton translational ion dynamics. This interpretation is fully corroborated by ^{1}H line shape measurements: we observe a complete motion-controlled narrowing curve of the NMR line widths that undoubtedly suggests effective and full averaging of homo- and heteronuclear dipole−dipole couplings through translational, that is, hopping, H^+ ion dynamics. Finally, the proton self-diffusion coefficient estimated at 125 °C directly from ^{1}H NMR ($D_H = 1.2 \times 10^{-15}$ m^2 s^{-1}, 0.45 eV) is comparable to other values presented in the literature for garnet-type ceramics but lower than those reported for the various $BaZrO_3$-based compounds containing protons.

ASSOCIATED CONTENT

Supporting Information

The Supporting Information is available free of charge at https://pubs.acs.org/doi/10.1021/acs.jpcc.3c02330.

Brief introduction into the basics of NMR relaxation, additional experimental details, and fitting results of the relaxation rate peaks (PDF)

AUTHOR INFORMATION

Corresponding Author

H. Martin R. Wilkening − *Institute of Chemistry and Technology of Materials (NAWI Graz), Graz University of Technology, 8010 Graz, Austria*; orcid.org/0000-0001-9706-4892; Email: wilkening@tugraz.at

Authors

Maria Gombotz − *Institute of Chemistry and Technology of Materials (NAWI Graz), Graz University of Technology, 8010 Graz, Austria*

Caroline Hiebl − *Institute of Chemistry and Technology of Materials (NAWI Graz), Graz University of Technology, 8010 Graz, Austria*

Florian Stainer − *Institute of Chemistry and Technology of Materials (NAWI Graz), Graz University of Technology, 8010 Graz, Austria*

Complete contact information is available at: https://pubs.acs.org/10.1021/acs.jpcc.3c02330

Notes

The authors declare no competing financial interest.

ACKNOWLEDGMENTS

We thank the Leibniz Institut für Kristallzüchtung (S. Ganschow, Berlin) for leaving us the LLZTO single crystals for further investigations and D. Rettenwander for discussions on sample preparation, that is, the Li/H exchange process. We appreciate financial support by the Deutsche Forschungsgemeinschaft (DFG, WI3600 (4-1)) and by the project safeLIB. safeLIB is a COMET (Competence Centers for Excellent Technologies) project managed by the FFG (Österreichische Forschungsförderungsgesellschaft).

REFERENCES

(1) Funke, K. Solid State Ionics: from Michael Faraday to green energy — the European dimension. *Sci. Technol. Adv. Mater.* **2013**, *14*, No. 043502.
(2) Knauth, P. Inorganic solid Li ion conductors: an overview. *Solid State Ion.* **2009**, *180*, 911−916.
(3) Tuller, H. L. Ionic conduction in nanocrystalline materials. *Solid State Ion.* **2000**, *131*, 143−157.
(4) Knauth, P.; Tuller, H. L. Solid-state ionics: roots, status, and future Prospects. *J. Am. Ceram. Soc.* **2002**, *85*, 1654−1680.
(5) Norby, T. Solid-state protonic conductors: principles, properties, progress and prospects. *Solid State Ion.* **1999**, *125*, 1−11.
(6) Fop, S. Solid oxide proton conductors beyond perovskites. *J. Mater. Chem. A* **2021**, *9*, 18836−18856.
(7) Bachman, J. C.; Muy, S.; Grimaud, A.; Chang, H.-H.; Pour, N.; Lux, S. F.; Paschos, O.; Maglia, F.; Lupart, S.; Lamp, P.; Giordano, L.; Shao-Horn, Y. Inorganic solid-state electrolytes for Lithium batteries: mechanisms and properties governing ion conduction. *Chem. Rev.* **2016**, *116*, 140−162.
(8) Thangadurai, V.; Narayanan, S.; Pinzaru, D. Garnet-type solid-state fast Li ion conductors for Li batteries: critical review. *Chem. Soc. Rev.* **2014**, *43*, 4714−4727.
(9) Zhang, Z.; Shao, Y.; Lotsch, B.; Hu, Y.-S.; Li, H.; Janek, J.; Nazar, L. F.; Nan, C.-W.; Maier, J.; Armand, M.; Chen, L. New horizons for inorganic solid state ion conductors. *Energy Environ. Sci.* **2018**, *11*, 1945−1976.
(10) Krauskopf, T.; Richter, F. H.; Zeier, W. G.; Janek, J. Physicochemical concepts of the Lithium metal anode in solid-state batteries. *Chem. Rev.* **2020**, *120*, 7745−7794.
(11) Uitz, M.; Epp, V.; Bottke, P.; Wilkening, M. Ion dynamics in solid electrolytes for lithium batteries. *J. Electroceram.* **2017**, *38*, 142−156.
(12) Hayashi, A.; Noi, K.; Sakuda, A.; Tatsumisago, M. Superionic glass-ceramic electrolytes for room-temperature rechargeable sodium batteries. *Nat. Commun.* **2012**, *3*, 856.
(13) Zhou, W.; Li, Y.; Xin, S.; Goodenough, J. B. Rechargeable sodium all-solid-state battery. *ACS Central Sci.* **2017**, *3*, 52−57.
(14) Ormerod, R. M. Solid oxide fuel cells. *Chem. Soc. Rev.* **2003**, *32*, 17−28.
(15) Devi, P. S.; Sharma, A. D.; Maiti, H. S. Solid oxide fuel cell materials: a review. *Trans. Ind. Ceram. Soc.* **2004**, *63*, 75−98.
(16) Adams, T. A.; Nease, J.; Tucker, D.; Barton, P. I. Energy Conversion with Solid Oxide Fuel Cell Systems: A Review of Concepts and Outlooks for the Short- and Long-Term. *Ind. Eng. Chem. Res.* **2013**, *52*, 3089−3111.
(17) Ye, R.; Ihrig, M.; Imanishi, N.; Finsterbusch, M.; Figgemeier, E. A Review on Li^+ /H^+ Exchange in Garnet Solid Electrolytes: From Instability against Humidity to Sustainable Processing in Water. *Chem. Sus. Chem.* **2021**, *14*, 4397−4407.
(18) Meng, Y.; Gao, J.; Zhao, Z.; Amoroso, J. W.; Tong, J.; Brinkman, K. S. Review: recent progress in low-temperature proton-conducting ceramics. *J. Mater. Sci.* **2019**, *54*, 9291−9312.
(19) Kreuer, K. Proton-Conducting Oxides. *Ann. Rev. Mater. Res.* **2003**, *33*, 333−359.

(20) Mather, G. C.; Islam, M. S. Defect and Dopant Properties of the $SrCeO_3$ -Based Proton Conductor. *Chem. Mater.* **2005**, *17*, 1736−1744.

(21) Ryu, K. H.; Haile, S. M. Chemical stability and proton conductivity of doped $BaCeO_3 - BaZrO_3$ solid solutions. *Solid State Ion.* **1999**, *125*, 355−367.

(22) Hibino, T.; Mizutani, K.; Yajima, T.; Iwahara, H. Characterization of proton in Y-doped $SrZrO_3$ polycrystal by IR spectroscopy. *Solid State Ion.* **1992**, *58*, 85−88.

(23) Bohn, H.; Schober, T.; Mono, T.; Schilling, W. The high temperature proton conductor $Ba_3\ Ca_{1.18}Nb_{1.82}O_{9-\delta}$. *Solid State Ion.* **1999**, *117*, 219−228.

(24) Norby, T.; Kofstad, P. Proton and native-ion conductivities in $Y_2\ O_3$ at high temperatures. *Solid State Ion.* **1986**, *20*, 169−184.

(25) Norby, T.; Dyrlie, O.; Kofstad, P. Protons in Ca-doped $La_2\ O_3$, Nd_2O_3 and $LaNdO_3$. *Solid State Ion.* **1992**, *53*−*56*, 446−452.

(26) Norby, T.; Dyrlie, O.; Kofstad, P. Protonic Conduction in Acceptor-Doped Cubic Rare-Earth Sesquioxides. *J. Am. Ceram. Soc.* **1992**, *75*, 1176−1181.

(27) Hinterberg, J.; Adams, A.; Blümich, B.; Heitjans, P.; Kim, S.; Munir, Z. A.; Martin, M. ^{1}H-NMR measurements of proton mobility in nano-crystalline YSZ. *Phys. Chem. Chem. Phys.* **2013**, *15*, 19825−19830.

(28) Yamazaki, Y.; Blanc, F.; Okuyama, Y.; Buannic, L.; Lucio-Vega, J.; Grey, C. P.; Haile, S. M. Proton trapping in yttrium-doped barium zirconate. *Nat. Mater.* **2013**, *12* (7), 647−51.

(29) Wang, L. S.; Patel, S. V.; Truong, E.; Hu, Y.-Y.; Haile, S. M. Phase Behavior and Superprotonic Conductivity in the System $(1 - x)CsH_2\ PO_4\ \text{-}x\ H_3\ PO_4$: Discovery of Off-Stoichiometric α-$[Cs_{1-x}\ H_x\ ]H_2\ PO_4$. *Chem. Mater.* **2022**, *34*, 1809−1820.

(30) Kim, G.; Griffin, J. M.; Blanc, F.; Haile, S. M.; Grey, C. P. Characterization of the Dynamics in the Protonic Conductor $CsH_2\ PO_4$ by ^{17}O Solid-State NMR Spectroscopy and First-Principles Calculations: Correlating Phosphate and Protonic Motion. *J. Am. Chem. Soc.* **2015**, *137*, 3867−3876.

(31) Kim, G.; Blanc, F.; Hu, Y.-Y.; Grey, C. P. Understanding the Conduction Mechanism of the Protonic Conductor $CsH_2\ PO_4$ by Solid-State NMR Spectroscopy. *J. Phys. Chem. C* **2013**, *117*, 6504−6515.

(32) Draber, F. M.; Ader, C.; Arnold, J. P.; Eisele, S.; Grieshammer, S.; Yamaguchi, S.; Martin, M. Nanoscale percolation in doped $BaZrO_3$ for high proton mobility. *Nat. Mater.* **2020**, *19*, 338−346.

(33) Böhmer, R.; Jeffrey, K.; Vogel, M. Solid-state Li NMR with applications to the translational dynamics in ion conductors. *Prog. Nucl. Magn. Reson. Spectrosc.* **2007**, *50*, 87−174.

(34) Wilkening, M.; Heitjans, P. From micro to macro: access to long-range Li^+ diffusion parameters in solids via microscopic ^{6,7}Li spin-alignment echo NMR spectroscopy. *ChemPhysChem* **2012**, *13*, 53−65.

(35) Kuhn, A.; Narayanan, S.; Spencer, L.; Goward, G.; Thangadurai, V.; Wilkening, M. Li self-diffusion in garnet-type $Li_7\ La_3\ Zr_2\ O_{12}$ as probed directly by diffusion-induced ^{7}Li spin-lattice relaxation NMR spectroscopy. *Phys. Rev. B* **2011**, *83*, No. 094302.

(36) Vinod Chandran, C.; Heitjans, P. In *Annual Reports on NMR Spectroscopy*; Webb, G. A., Ed.; Academic Press: London, 2016; Vol. *89*; Chapter Solid-state NMR studies of lithium ion dynamics across materials classes, pp 1−102.

(37) Redhammer, G. J.; Badami, P.; Meven, M.; Ganschow, S.; Berendts, S.; Tippelt, G.; Rettenwander, D. Wet-Environment-Induced Structural Alterations in Single- and Polycrystalline LLZTO Solid Electrolytes Studied by Diffraction Techniques. *ACS Appl. Mater. Interface* **2021**, *13*, 350−359.

(38) Murugan, R.; Thangadurai, V.; Weppner, W. Fast Lithium Ion Conduction in Garnet-Type $Li_7\ La_3\ Zr_2\ O_{12}$. *Angew. Chem. Inten. Ed.* **2007**, *46*, 7778−7781.

(39) Liu, Q.; Geng, Z.; Han, C.; Fu, Y.; Li, S.; He, Y.; Kang, F.; Li, B. Challenges and perspectives of garnet solid electrolytes for all solid-state lithium batteries. *J. Power Sources* **2018**, *389*, 120−134.

(40) Cheng, L.; et al. The origin of high electrolyte-electrode interfacial resistances in lithium cells containing garnet type solid electrolytes. *Phys. Chem. Chem. Phys.* **2014**, *16*, 18294−18300.

(41) Hofstetter, K.; Samson, A. J.; Narayanan, S.; Thangadurai, V. Present understanding of the stability of Li-stuffed garnets with moisture, carbon dioxide, and metallic lithium. *J. Power Sources* **2018**, *390*, 297−312.

(42) Uhlenbruck, S.; Dellen, C.; Müller, S.; Lobe, S.; Tsai, C.-L.; Finsterbusch, M.; Bram, M.; Guillon, O. Reactions of garnet-based solid-state lithium electrolytes with water - A depth-resolved study. *Solid State Ion.* **2018**, *320*, 259−265.

(43) Galven, C.; Dittmer, J.; Suard, E.; Le Berre, F.; Crosnier-Lopez, M.-P. Instability of Lithium Garnets against Moisture. Structural Characterization and Dynamics of $Li_{7-x}\ H_x\ La_3\ Sn_2\ O_{12}$ and $Li_{5-x}\ H_x\ La_3\ Nb_2\ O_{12}$. *Chem. Mater.* **2012**, *24*, 3335−3345.

(44) Galven, C.; Fourquet, J.-L.; Crosnier-Lopez, M.-P.; Le Berre, F. Instability of the Lithium Garnet $Li_7\ La_3\ Sn_2\ O_{12}$: Li^+ /H^+ Exchange and Structural Study. *Chem. Mater.* **2011**, *23*, 1892−1900.

(45) Liu, C.; Rui, K.; Shen, C.; Badding, M. E.; Zhang, G.; Wen, Z. Reversible ion exchange and structural stability of garnet-type Nb-doped $Li_7\ La_3\ Zr_2\ O_{12}$ in water for applications in lithium batteries. *J. Power Sources* **2015**, *282*, 286−293.

(46) Truong, L.; Howard, M.; Clemens, O.; Knight, K. S.; Slater, P. R.; Thangadurai, V. Facile proton conduction in H^+ /Li^+ ion-exchanged garnet-type fast Li-ion conducting $Li_5\ La_3\ Nb_2\ O_{12}$. *J. Mater. Chem. A* **2013**, *1*, 13469−13475.

(47) Truong, L.; Thangadurai, V. Soft-Chemistry of Garnet-Type $Li_{5+x}\ Ba_x\ La_{3-x}\ Nb_2\ O_{12}$ (x = 0,0.5,1): Reversible $H^+ \leftrightarrow Li^+$ Ion-Exchange Reaction and Their X-ray, ^{7}Li MAS NMR, IR, and AC Impedance Spectroscopy Characterization. *Chem. Mater.* **2011**, *23*, 3970−3977.

(48) Truong, L.; Thangadurai, V. First Total H^+/Li^+ Ion Exchange in Garnet-Type $Li_5La_3Nb_2O_{12}$ Using Organic Acids and Studies on the Effect of Li Stuffing. *Inorg. Chem.* **2012**, *51*, 1222−1224.

(49) Yow, Z. F.; Oh, Y. L.; Gu, W.; Rao, R. P.; Adams, S. Effect of Soft-Chemistry of Garnet-Type $Li_{5+x}Ba_xLa_{3-x}Nb_2O_{12}$ (x = 0,0.5, 1): Reversible H^+/Li^+ Ion-Exchange Reaction and Their X-ray, 7Li MAS NMR, IR, and AC Impedance Spectroscopy Characterization exchange in water treated Ta-doped $Li_7La_3Zr_2O_{12}$. *Solid State Ion.* **2016**, *292*, 122−129.

(50) Li, Y.; Han, J.-T.; Vogel, S. C.; Wang, C.-A. The reaction of $Li_{6.5}\ La_3\ Zr_{1.5}\ Ta_{0.5}\ O_{12}$ with water. *Solid State Ion.* **2015**, *269*, 57−61.

(51) Galven, C.; Suard, E.; Mounier, D.; Crosnier-Lopez, M.-P.; Le Berre, F. Structural characterization of a new acentric protonated garnet: $Li_{6-x}\ H_x\ CaLa_2\ Nb_2\ O_{12}$. *J. Mater. Res.* **2013**, *28*, 2147−2153.

(52) Orera, A.; Larraz, G.; Rodríguez-Velamazmazán, J. A.; Campo, J.; Sanjuán, M. L. Influence of Li^+ and H^+ Distribution on the Crystal Structure of $Li_{7-x}H_xLa_3Zr_2O_{12}$ ($0 < x < 5$) Garnets. *Inorg. Chem.* **2016**, *55*, 1324−1332.

(53) Hiebl, C.; Young, D.; Wagner, R.; Wilkening, H. M. R.; Redhammer, G. J.; Rettenwander, D. Proton Bulk Diffusion in Cubic $Li_7\ La_3\ Zr_2\ O_{12}$ Garnets as Probed by Single X-ray Diffraction. *J. Phys. Chem. C* **2019**, *123*, 1094−1098.

(54) Shimonishi, Y.; Toda, A.; Zhang, T.; Hirano, A.; Imanishi, N.; Yamamoto, O.; Takeda, Y. Synthesis of garnet-type $Li_{7-x}\ La_3\ Zr_2\ O_{12-(1/2)x}$ and its stability in aqueous solutions. *Solid State Ionics* **2011**, *183*, 48−53.

(55) Gam, F.; Galven, C.; Bulou, A.; Le Berre, F.; Crosnier-Lopez, M.-P. Reinvestigation of the Total Li^+ /H^+ Ion Exchange on the Garnet-Type $Li_5\ La_3\ Nb_2\ O_{12}$. *Inorg. Chem.* **2014**, *53*, 931−934.

(56) Brugge, R. H.; Hekselman, A. K. O.; Cavallaro, A.; Pesci, F. M.; Chater, R. J.; Kilner, J. A.; Aguadero, A. Garnet Electrolytes for Solid State Batteries: Visualization of Moisture-Induced Chemical Degradation and Revealing Its Impact on the Li-Ion Dynamics. *Chem. Mater.* **2018**, *30*, 3704−3713.

(57) Stanje, B.; Rettenwander, D.; Breuer, S.; Uitz, M.; Berendts, S.; Lerch, M.; Uecker, R.; Redhammer, G.; Hanzu, I.; Wilkening, M. Solid Electrolytes: Extremely Fast Charge Carriers in Garnet-Type $Li_6\ La_3\ ZrTaO_{12}$ Single Crystals. *Ann. Phys. (Berlin)* **2017**, *529*, 1700140.

https://doi.org/10.1021/acs.jpcc.3c02330
J. Phys. Chem. C 2023, 127, 10960−10967

(58) Epp, V.; Gün, O.; Deiseroth, H.-J.; Wilkening, M. Long-range Li^+ dynamics in the lithium argyrodite Li_7PSe_6 as probed by rotating-frame spin-lattice relaxation NMR. *Phys. Chem. Chem. Phys.* **2013**, *15*, 7123−7132.
(59) Gombotz, M.; Wilkening, H. M. R. Fast Li Ion Dynamics in the Mechanosynthesized Nanostructured Form of the Solid Electrolyte Li_3YBr_6. *ACS Sust. Chem. Engin.* **2021**, *9*, 743−755.
(60) Posch, P.; Lunghammer, S.; Berendts, S.; Ganschow, S.; Redhammer, G. J.; Wilkening, A.; Lerch, M.; Gadermaier, B.; Rettenwander, D.; Wilkening, H. M. R. Ion dynamics in Al-Stabilized $Li_7La_3Zr_2O_{12}$ single crystals − Macroscopic transport and the elementary steps of ion hopping. *Energy Storage Mater.* **2020**, *24*, 220−228.
(61) Bloembergen, N.; Purcell, E. M.; Pound, R. V. Relaxation effects in Nuclear Magnetic Resonance absorption. *Phys. Rev.* **1948**, *73*, 679−712.
(62) Hogrefe, K.; Minafra, N.; Zeier, W. G.; Wilkening, H. M. R. Tracking Ions the Direct Way: Long-Range Li^+ Dynamics in the Thio-LISICON Family Li_4MCh_4 (M = Sn, Ge; Ch = S, Se) as Probed by ^{7}Li NMR Relaxometry and ^{7}Li Spin-Alignment Echo NMR. *J. Phys. Chem. C* **2021**, *125*, 2306−2317.
(63) Ingram, M. In *Encyclopedia of Materials: Science and Technology*; Buschow, K. J., Cahn, R. W., Flemings, M. C., Ilschner, B., Kramer, E. J., Mahajan, S., Veyssière, P., Eds.; Elsevier: Oxford, 2001; pp 220−223.
(64) Cramer, C.; Brückner, S.; Gao, Y.; Funke, K. Ion dynamics in mixed alkali glasses. *Phys. Chem. Chem. Phys.* **2002**, *4*, 3214−3218.
(65) Faske, S.; Koch, B.; Murawski, S.; Küchler, R.; Böhmer, R.; Melchior, J.; Vogel, M. Mixed-cation $Li_xAg_{1-x}PO_3$ glasses studied by ^{6}Li, ^{7}Li, and ^{109}Agstimulated-echo NMR spectroscopy. *Phys. Rev. B* **2011**, *84*, No. 024202.
(66) Wilkening, M.; Bork, D.; Indris, S.; Heitjans, P. Diffusion in amorphous $LiNbO_3$ studied by ^{7}Li NMR − Comparison with the nano- and microcrystalline material. *Phys. Chem. Chem. Phys.* **2002**, *4*, 3246−3251.
(67) Smetaczek, S.; Limbeck, A.; Zeller, V.; Ring, J.; Ganschow, S.; Rettenwander, D.; Fleig, J. Li^+ /H^+ exchange of $Li_7La_3Zr_2O_{12}$ single and polycrystals investigated by quantitative LIBS depth profiling. *Mater. Adv.* **2022**, *3*, 8760−8770.
(68) Kreuer, K.; Adams, S.; Münch, W.; Fuchs, A.; Klock, U.; Maier, J. Proton conducting alkaline earth zirconates and titanates for high drain electrochemical applications. *Solid state ion.* **2001**, *145*, 295−306.
(69) Kreuer, K.; Dippel, T.; Baikov, Y.; Maier, J. Water solubility, proton and oxygen diffusion in acceptor doped $BaCeO_3$,: a single crystal analysis. *Solid State Ion.* **1996**, *86*−*88*, 613−620.
(70) Oishi, M.; Akoshima, S.; Yashiro, K.; Sato, K.; Mizusaki, J.; Kawada, T. Defect structure analysis of B-site doped perovskite-type proton conducting oxide $BaCeO_3$ Part 2: the electrical conductivity and diffusion coefficient of $BaCe_{0.9}Y_{0.1}O_{3-\delta}$. *Solid State Ion.* **2008**, *179*, 2240−2247.
(71) Kreuer, K.; Schönherr, E.; Maier, J. Proton and oxygen diffusion in $BaCeO_3$ based compounds: a combined thermal gravimetric analysis and conductivity study. *Solid State Ion.* **1994**, *70* (71), 278−284.
(72) Wei, T.; Zhang, L.; Chen, Y.; Yang, P.; Liu, M. Promising Proton Conductor for Intermediate-Temperature Fuel Cells: $Li_{13.9}Sr_{0.1}Zn(GeO_4)_4$. *Chem. Mater.* **2017**, *29*, 1490−1495.

https://doi.org/10.1021/acs.jpcc.3c02330
J. Phys. Chem. C 2023, 127, 10960−10967